Article

Journal of the Brazilian Chemical Society

https://dx.doi.org/10.21577/0103-5053.20240072

J. Braz. Chem. Soc. **2024**, *35*, 11, e-20240072, 1-11

Investigating Solid-State Luminescent Properties of New Cadmium(II) and Lead(II) Oxamato-Based Coordination Polymers

Jhonny W. Maciel,[a] Jackson Junior S. de Souza,[a] Ana K. Valdo,[b] Felipe T. Martins,[a] Freddy F. Guimarães,[a] Ricardo C. de Santana,[c] *, *Lauro J. Q. Maia[c] and Danielle Cangussu*[a]*

[a]*Instituto de Química, Universidade Federal de Goiás, 74690-900 Goiânia-GO, Brazil,*

[b]*Instituto Federal Goiano, Campus Iporá, 76200-000 Goiânia-GO, Brazil*

[c]*Instituto de Física, Universidade Federal de Goiás, 74690-900 Goiânia-GO, Brazil*

Two novel coordination polymers were synthesized through the reaction of the $Hpcpa^{2-}$ ligand (H_3pcpa = *N*-(4-carboxyphenyl)oxamic acid) with cadmium(II) and lead(II) metal ions, yielding $[Cd_2(Hpcpa)_2(H_2O)_6]_n \cdot H_2O$ (**1**) and $[Pb(Hpcpa)(H_2O)]_n$ (**2**). Structural analysis by single-crystal X-ray diffraction revealed that **1** consists of one-dimensional zigzag polymeric chains, while **2** is a three-dimensional polymer network. Additionally, investigations of their optical properties were carried out in a comparative study involving the previously reported pcpa-based coordination polymers $\{[Zn(Hpcpa)(H_2O)_3] \cdot 0.5H_2O\}_n$ and $\{[Gd_2(Hpcpa)_3(H_2O)_5] \cdot H_2O\}_n$], called here as **3** and **4**, respectively. Under 330 nm excitation wavelength, all compounds exhibited broad emission bands spanning from 350 to 650 nm. Particularly, **1** and **3** displayed notable external quantum yields of 15.4 and 12.8%, respectively, highlighting their potential in luminescent applications.

Keywords: coordination polymers, luminescence, oxamato

Introduction

This is the golden age of materials. Every day new materials are actively developed to face the increasing demand of society for more adaptive approaches that can remodel our benefit: improved quality of life, better healthcare, environmental solutions, energy and time efficiencies, and lower manufacturing costs. To address those demands and their rapid scaling, molecular materials appear as game-changers in improving the performance, utilization and miniaturization of the materials thanks to their outstanding versatility. Those features consist in a crucial point to conceive the products of the future, leading to a new upcoming period of humankind: The Molecular Age.

In this respect, coordination polymers (CPs) constitute an important class of molecular materials that combine structural and physical-chemical properties.[1,2] No wonder CPs have attracted much attention in recent years for many applications (processes) covering gas storage,[3,4] gas separation,[5-7] catalysis,[8-10] environmental remediation,[11-13] energy harvesting,[14,15] and chemical sensing.[16-18] In fact, most applications of CPs are in molecule absorption, storage and separation[3,7,19] while their electronic features are still a meagre field, and the first examples of luminescent[20-22] CPs were only recently reported.

The rational arrangement of π-conjugated organic moieties in a periodic lattice enabled the control of energy transfer processes (antenna effect),[23-27] turning the material into a sensor for exogenous molecules that modify the luminescence.[16,18] Besides this organic approach, metal-based luminescence was also used to incorporate functionality into the material. This fact is well exemplified by the lanthanide-based CPs, a family of materials known for their luminescence phenomena occurring in the visible range of the spectrum. These compounds exhibit many applications, including medical imaging,[28,29] luminescent thermometers,[30-34] white light-emitting compounds,[35,36] and optical sensors.[37-40]

With this purpose, aromatic oxamato ligands have been widely used to obtain luminescent CPs with 3d and 4f metal ions. The greatest advantage of this type of ligand is the ability to build CPs with predictable structures[41-43] and tuneable properties. Our group has been exploring the

*e-mail: danielle_cangussu@ufg.br; santana@ufg.br
Editor handled this article: Ítalo O. Mazali (Guest)
In honor of Professor Oswaldo, whose unwavering dedication to scientific research, mentorship and heartfelt passion for chemistry continue to inspire us all.

coordination chemistry of oxamato ligands, particularly of the *N*-(4-carboxyphenyl)oxamic acid (H_3pcpa),[44-46] a ligand that afforded a new class of CPs of transition metal. This ligand proved to be effective in binding first-row transition metal ions such as Co(II), Mn(II), Zn(II) and lanthanide Eu(III), Gd(III) and Tb(III) ions, leading to CPs of formula $\{[M(Hpcpa)(H_2O)_3]\cdot 0.5H_2O\}_n$, and $\{[Ln_2(Hpcpa)_3(H_2O)_5]\cdot H_2O\}_n$. Motivated by our previous works, we were driven to investigate the capability of the H_3pcpa ligand to interact with metal ions commonly pointed as environmental threads on aquatic ecosystems, resulting in insoluble CPs. Herein, we report the synthesis, structural and spectroscopic characterization, and optical properties of two novel coordination polymers based on Cd(II) (**1**) or Pb(II) (**2**) and the pcpa ligand obtained in the form of both single-crystals and polycrystalline samples.

Experimental

General information

All chemicals were of reagent-grade quality, purchased from commercial sources (Sigma-Aldrich, Saint Louis, USA) and used without further purification. The synthesis of the proligand *N*-(4-carboxyphenyl)oxamic acid (EtH_2pcpa) and its corresponding deprotonated sodium salt of formula $Na_2Hpcpa\cdot xH_2O$ followed previous reports.[45,46] Elemental analyses (Thermo Scientific™ FLASH 2000 CHNS/O Analyzers, Waltham, Massachusetts, USA), infrared (Spectrum 400, PerkinElmer, Waltham, Massachusetts, USA) and electronic spectrum (Lambda 45, PerkinElmer, Waltham, Massachusetts, USA) were performed at Central de Análises Multiusuária (CAM) of Universidade Federal de Goiás. Infrared spectra were recorded on powdered samples of **1** and **2** as KBr pellets. The electronic absorption spectrum of $Na_2Hpcpa\cdot xH_2O$ was recorded in aqueous solution ($c_M = 1.0 \times 10^{-5}$ M) at room temperature with a PerkinElmer UV/Vis/NIR spectrophotometer (Walthan, USA). ^{1}H NMR spectrum of $Na_2Hpcpa\cdot xH_2O$ (Figure S1, Supplementary Information (SI) section) was recorded at room temperature on a Bruker AC 500 (500 MHz) spectrometer (Billerica, Massachusetts, USA) by using deuterium oxide as a solvent and internal standard (δ = 4.80 ppm). Found signals (D_2O; 500 MHz, ppm) 7.55 (d, 2H, *J* 8.7 Hz) and 7.83 (d, 2H, *J* 8.7 Hz). The thermogravimetric analysis (TGA) was performed on powdered samples of **1** and **2** under a synthetic air atmosphere within the range of 30-650 °C with a Netzsch STA 449 F3 Nevio Nevio (NETZSCH-Gerätebau, Selb, Germany) thermobalance operating at a heating rate of 10 °C min^{-1}. Powder X-ray diffraction (PXRD) data were collected for polycrystalline powders of **1** and **2** in a Bruker D8 Discover (Bruker, Billerica, Massachusetts, USA) powder diffractometer, using Cu Kα radiation (λ = 1.54177 Å) at a voltage of 40 kV and a current of 40 mA in the 2θ range 5.00-50.00° with step-size of 0.01° by Centro Regional para o Desenvolvimento Tecnológico e Inovação (CRTI) of Universidade Federal de Goiás.

Synthesis of $[Cd_2(Hpcpa)_2(H_2O)_6]_n\cdot H_2O$ (**1**) and $[Pb(Hpcpa)(H_2O)]_n$ (**2**)

Compounds **1** and **2** were prepared by a mixture of an aqueous solution of Na_2Hpcpa (0.3 mmol, 0.076 g) and an aqueous solution of $Cd(NO_3)_2\cdot 4H_2O$ (0.3 mmol, 0.098 g) and $Pb(NO_3)_2$ (0.3 mmol, 0.099 g) on the other side. Yield: 80% (**1**) and 86% (**2**). Anal. calcd. for $C_{18}H_{24}Cd_2N_2O_{17}$ (**1**): C 28.24; H, 3.13; N, 3.66. Found: C 28.93; H, 3.12; N, 3.52%. Anal. calcd. for $C_9H_7NO_6Pb$ (**2**): C, 25.00; H, 1.62; N, 3.24. Found: C, 26.90; H, 1,22; N, 3.38%. Selected IR data (KBr) ν / cm^{-1} 3438, 3325, 1677, 1654, 1520, 1410, for **1**; 3430, 3320, 1673, 1661, 1533, 1497, for **2**. The colorless needle-like crystals of **1** and **2** were obtained by slow diffusion in H-shaped tube with an aqueous solution of Na_2Hpcpa (0.1 mmol, 0.037 g) placed on one side of the tube and an aqueous solution of $Cd(NO_3)_2\cdot 4H_2O$ (0.1 mmol, 0.0308 g) and $Pb(NO_3)_2$ (0.1 mmol, 0.0331 g) on the other side after standing at room temperature for five days.

Crystallographic data collection and refinement

Room temperature intensity data were collected on a Bruker-AXS Kappa Duo diffractometer (Billerica, USA) equipped with an APEX II CCD detector with either Cu Kα (λ = 1.54178 Å, compound **1**) or Mo Kα (λ = 0.71073 Å, compound **2**). Multi-scan absorption correction was applied to both raw datasets, with ratio between the minimum and maximum transmission factors of 0.822 and 0.923 for **1** and **2**, respectively. The structures were solved with SHELXS and refined with SHELXL-2018.[47] Isotropic displacement parameters were used for hydrogens and were 20% higher than the equivalent isotropic displacement (Ueq) values of the bonded carbon or nitrogen. This value was 50% in the case of water hydrogens. The hydrogens were initially positioned taking into consideration both intramolecular features and intermolecular surroundings and then their positions were constrained following a riding model (except for water hydrogens, which were first localized from the difference Fourier map and then fixed without further oscillation). The structure analyses and drawings were performed with MERCURY[48] and ORTEP-3[49] programs.

A summary of the single crystal X-ray diffraction intensity collection experiment and the crystal data treatment is shown in Table 1. It is worth to mention that crystals of compound **1** have presented poor quality, diffracting with low intensity even at medium resolution shell and with some twinning, which resulted in a somewhat large symmetry factor (Rint) and low completeness reported in Table 1. Also in **1**, large residual electronic density peaks were found near to the transition metal ion site.

Optical measurements

Diffuse reflectance spectra were measured in a PerkinElmer Lambda WB1050 spectrometer (Waltham, USA) equipped with a Praying Mantis diffuse reflection accessory in the range of 250-1300 nm at room temperature. Photoluminescence (PL) emission spectra of the solid samples were measured using a Horiba-Jobin Yvon spectrofluorimeter, Model Fluorolog-3 (FL3-221), under excitation with a 450 W Xe lamp and Hamamatsu photomultiplier photon detector in the UV-Vis region. The excitation and emission bandpass were 1.0 nm. PL emission was corrected for the spectral response of the monochromators and the detector using a typical correction spectrum provided by the manufacturer. Quantum yields (QY) were acquired using an integrating sphere (Quanta-ϕ equipment, F3029, Horiba Jobin Yvon, New Jersey, USA) of Spectralon® coupled employing optical fibers. The internal and external quantum yields (iQY and eQY) were calculated following the method developed by Wrighton *et al.*[50] where iQY (%) = $(E_s/(L_{std} - L_s)) \times 100$, where E_s the number of emitted photons from the sample, L_{std} and L_s the number of reflected photons from the reflection standard and from the sample, respectively, with $(L_{std} - L_s)$ being the number of photons absorbed by the sample. The external QY (eQY (%) = $L_s/L_{std} \times 100$) is the ratio between the number of emitted photons from the sample and the number of reflected photons from the

Table 1. Crystal data and refinement parameters for compounds **1** and **2**

Compound		**1**	**2**
Chemical formula		$C_{18}H_{24}Cd_2N_2O_{17}$	$C_9H_7NO_6Pb$
Crystal system		monoclinic	monoclinic
Space group		$P2_1/c$	$P2_1/c$
Z		4	4
Unit cell dimension	a / Å	7.4735(2)	12.6456(5)
	b / Å	26.5285(6)	6.7550(3)
	c / Å	12.6707(3)	12.8100(5)
	β / degree	91.1390(10)	108.491(2)
Volume / Å^3		2511.61(11)	1037.75(7)
Density$_{calc.}$ / (g cm^{-3})		2.024	2.767
Absorption coefficient / (μ mm^{-1})		14.357 (Cu Kα)	16.275 (Mo Kα)
Theta range for data collection (θ) / degree		3.332-66.347	1.698-25.051
Index range	h	–8 to 8	–14 to 15
	k	–29 to 31	–7 to 8
	l	–10 to 14	–15 to 15
Data collected/Unique reflections / $I > 2\sigma(I)$		11318/4246/3652	11079/1831/1737
Symmetry factor (R_{int})		0.1035	0.0497
Completeness to θ_{max} / %		96.3	99.8
F(000)		1512	792
Refined parameters		352	154
Goodness-of-fit on F^2(*S*)		1.003	1.049
Final R_1 factor [$I > 2\sigma(I)$]		0.0702	0.0173
wR_2 factor (all data)		0.1839	0.0447
Largest diff. peak/hole / (*e* Å^{-3})		3.238/-1.658	0.871/-0.812
CCDC deposit No.		2102736	2102735

a,b,c,α,β: unit cell parameters; *Z*: formula unit *per* unit cell; F(000): structure factor in the zeroth-order case; F^2 : squared structure factor; wR_2: R-value for F^2 ; CCDC: Cambridge Crystallographic Data Centre.

reflection standard, i.e., the total number of photons incident over the sample. This method is accurate within 10% of the measured values.[50] The luminescence decay curves were measured by using a pulse light from a nanoled as excitation source at 340 nm (ca. 1 ns width pulses and 1 MHz frequency) and a Horiba PPD-850 picosecond photon. The CIE1931 (x,y)[51] color coordinates and the respective color diagram were calculated from the luminescence spectra. All optical measurements were recorded at room temperature using finely ground powders.

Computational details

The full geometry optimization of the ligand was computed by the density functional theory (DFT) method in water as solvent followed by the frequency analysis of the normal modes in the same medium. The normal mode frequency analysis reported only real positive numbers for vibrational frequencies, ensuring the location of a minimum in the potential energy surface. The water solvent was simulated by polarizable continuum model (PCM).[52] The time-dependent density functional theory (TD-DFT) within the frame of PCM water solvent was also applied to compute the transition energies and the oscillator strengths that can be related to the absorption spectra. In the TD-DFT calculations, 70 electronic excitations to singlet excited states were considered. The exchange correlation function M062-x[53] and the Def2-TZVP[54,55] basis set were employed in both DFT and TD-DFT calculation. All calculations were performed by Gaussian 16 software.[56] The molecular system used in the electronic structure calculations was based on the double deprotonated $Hpcpa^{2-}$ dianion, in which there are no protons bonded to the oxygen atoms of the ligand.

Results and Discussion

Synthesis and characterizations

The slow diffusion in an H-shaped tube proved to be a good methodology to obtain single-crystals of coordination polymers with metal ions with the proligand [*N*-(4-carboxyphenyl)oxamic acid (H_3pcpa)].[44,45] On the other hand, the polycrystalline samples were obtained by mixing aqueous solutions of the stoichiometric amounts of the corresponding reagents. Indeed, the PXRD patterns of the polycrystalline samples (Figures S2a and S2b, SI section) are identical to the calculated ones from the single-crystal XRD analysis, confirming a pure crystalline phase of the bulk materials. The polycrystalline compounds of Zn(II) and Gd(III), named here as **3** and **4**, were obtained as described in the literature.[45,46]

The infrared spectra of **1** and **2** (Figures S3a and S3b, SI section) are similar. They show broad absorptions centered at 3438 and 3430 cm^{-1}, respectively, due to ν(O–H) from the hydrogen-bonded water molecules. The slight shifts of the ν(COO) characteristic frequencies centered at 1678 and 1654 (**1**), and 1673 and 1661 cm^{-1} (**2**) compared to those of the $Na_2Hpcpa{\cdot}xH_2O$ (1679 and 1648 cm^{-1}, Figure S4, SI section) are expected since the carboxylate groups are already involved in coordination interactions with metal ions in the sodium salt of the ligand.

The TGA (thermogravimetric analysis) profiles of **1** and **2** (Figures S5a and S5b, SI section) show that the compounds are stable up to 300 °C. Compound **1** exhibits a first loss of 13.5%, which can be attributed to a non-coordinated water molecule and six coordinated water molecules by an endothermic process observed in the DSC graph occurring between 74 and 109 °C. Differently, compound **2** does not show water loss up to 300 °C because the powdered samples in this case were vacuum dried and this proceeded to remove this molecule. The differences observed in the elemental analysis values and in the PDRX partner of **2** corroborate this result. Then, a nearly plateau is observed until around 300 °C, where losses related to ligand degradation occur through two exothermic processes seen in the DSC in the temperature ranges between 364-427 (**1**) and 374-472 °C (**2**). From this temperature, the final residues of thermal decomposition can be attributed to the formation of the respective metal oxides (CdO and PbO).

Structural descriptions

Compounds **1** and **2** crystallize in the $P2_1/c$ space group of the monoclinic system. However, the asymmetric unit in **1** consists of two Cd(II) ions, two $Hpcpa^{2-}$ ligands, six coordinated water molecules and another non-coordinated one (one lattice water), whereas in **2** there is only one Pb(II) ion, one $Hpcpa^{2-}$ ligand and one coordinated water molecule. In both compounds, each $Hpcpa^{2-}$ ligand is present with two carboxylate groups while the nitrogen atom from the oxamate moiety remains protonated. The overall backbone of the two crystallographically independent ligand molecules in **1** and **2** is close to planarity root-mean square deviation (RMSD) for all fifteen non-hydrogen ligand atoms fitted onto the molecular least-square plane is 0.289 and 0.149 Å for ligands labelled as A and B in **1** and 0.0920 Å in **2**. Notably, ligand A in **1** is more twisted than others reported here, which is a consequence of its higher torsion angles between the phenyl and oxamate (8.1 (ligand A, **1**), 3.6 (ligand B, **1**) and 1.8° (**2**)), and the phenyl and carboxylate moieties (8.7 (ligand A, **1**), 6.2 (ligand B, **1**) and 1.8° (**2**)). Both Cd(II)

and Pb(II) ions are seven-coordinated. While Cd1 is bonded to two oxamate oxygen atoms from ligands A and B, Cd2 is bonded to the two oxygen atoms of their carboxylate groups at the *para*-position. In both crystallographically independent Cd(II) ions, one water molecule is coordinated near the ligands oxygen atoms, forming a distorted basal plane of a pentagonal bipyramidal geometry (RMSD for the basal plane atoms Cd1, O2A, O3A, O2B, O3B and O3WA is 0.224 Å, and 0.225 Å for the basal least-square plane calculated through the atoms Cd2, O4A, O5A, O4B, O5B and O3WB) which is completed with other two water molecules bonded at the axial positions (O1WA and O2WA for Cd1; O1WB and O2WB for Cd2; coordination bonds and angles are listed in Table S1, SI section). Such coordination pattern gives rise to the main feature of the **1**, which is the formation of one-dimensional zigzag fashioned polymeric chains along the c-axis (Figures 1 and 2).

The intra-chain stability is also achieved from classical hydrogen bonds involving water molecules (see Table S2, SI section for interactions metrics), which also cross-link different chains packed on top of each other. On the other hand, Pb(II) adopts a capped trigonal antiprismatic geometry in **2** described in this study, with the coordinated water oxygen at the capping. All five oxygen atoms from the ligand are coordinated to Pb(II), and one of them is bidentate (O1; Figure 3). Differently from **1**, a three-dimensional polymeric network is assembled when the $Hpcpa^{2-}$ ligand reacts with Pb(II) ions (Figure 4) with

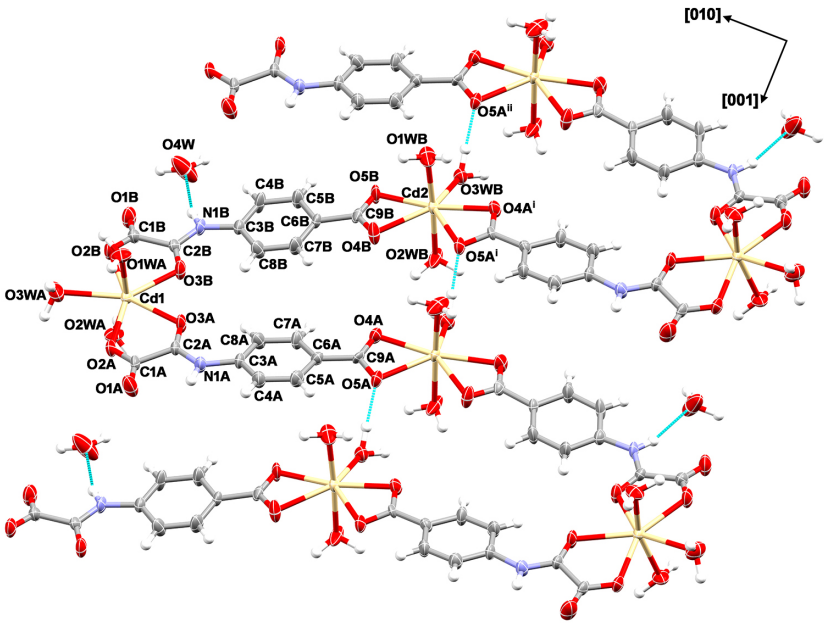

Figure 1. The one-dimensional coordination polymer formed in the crystal structure of **1**. Non-hydrogen and hydrogen atoms are drawn as 50% probability ellipsoids and arbitrary radius spheres, respectively. All non-hydrogen atoms in the asymmetric unit were labelled. Cyan dashed lines illustrate hydrogen bonds (the O–H···O intra-chain ones and those involving the amine group and the lattice water). The atom labels with a superscript letter do not belong to the asymmetric unit and were generated by symmetry: (i) x, ½–*y*, –½+*z*; (ii) *x*, *y*, –1+*z*.

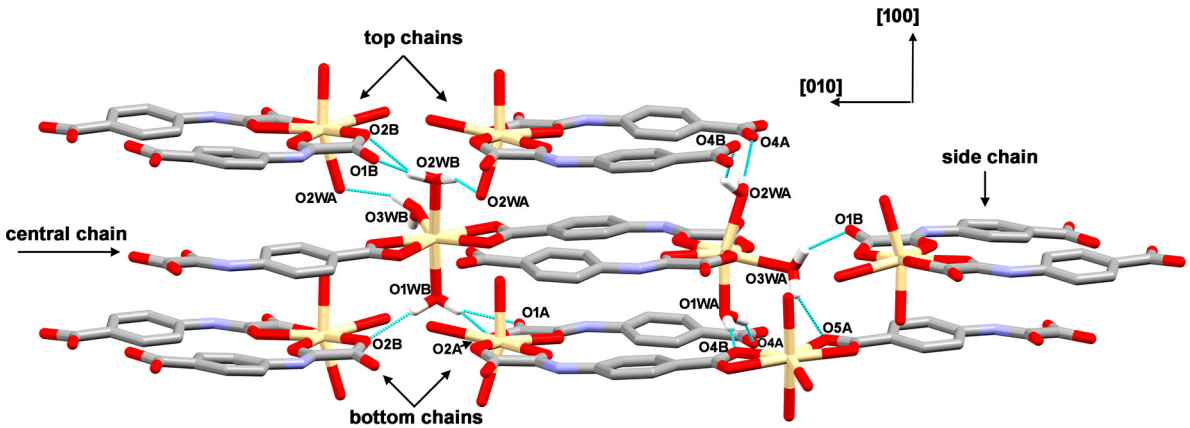

Figure 2. The role of inter-chain hydrogen bonds (cyan dashed lines) in the crystal structure of **1**.

classical hydrogen bonds involving the unique water molecule (see Table S2, SI section).

Optical results and theoretical calculations

Figure 5 depicts the experimental and theoretical UV-Vis absorption spectra of the ligand in water. The black dashed line represents the UV-Vis experimental results, which shows a narrow absorption band with a maximum at 271.9 nm as the lowest electronic transition energy in the UV-Vis region. The red continuous line is the convoluted theoretical absorption spectra computed by TD-DFT transition frequencies (wavelengths) and oscillator strengths (absorbance intensity), which are shown by red bars under the absorption bands. The convolution of the bar spectra was made by a Gaussian function with a full width at half maximum of 30 nm. The full theoretical spectrum was redshifted by 25 nm to a better comparison with the experimental one. The first forbidden electronic excitation in the TD-DFT calculation appears in 247.8 nm with the main contribution given by the transition from the highest occupied molecular orbital (HOMO) to the lowest unoccupied molecular orbital (LUMO). The inset a in Figure 5 represents the electron transition between these molecular orbitals that are responsible for the experimental absorption band in 271.9 nm. The TD-DFT suggests that the narrow band occurs due to a single HOMO-LUMO contribution to the transition with an oscillator strength of 0.6438 a.u. because all other electronic transitions in this energy region are prohibited or almost prohibited. An example is the HOMO-LUMO+1 transition in 242.4 nm which has very small oscillator strength (0.0164 a.u.) implying little effect in the lowest energy absorption band. The full-range experimental UV-Vis spectrum record

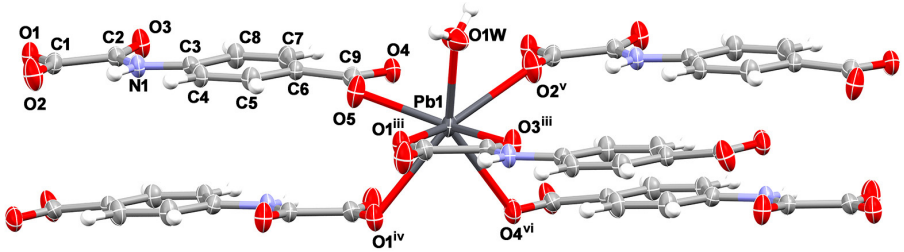

Figure 3. Perspective view of the crystallographic independent Pb(II) ions with its coordination sphere in **2**. Ellipsoids are drawn with 50% of probability for the non-hydrogen atoms of **2** (hydrogens are pictured as arbitrary radius spheres). All non-hydrogen atoms which are asymmetric units were labelled without superscript letters. Symmetry codes: (iii) –1+x, ½–*y*, –½+*z*; (iv) 2–*x*, –½+*y*, ½–*z*; (v) –1+x, y, *z*; (vi) 1–x, –½+*y*, ½–*z*.

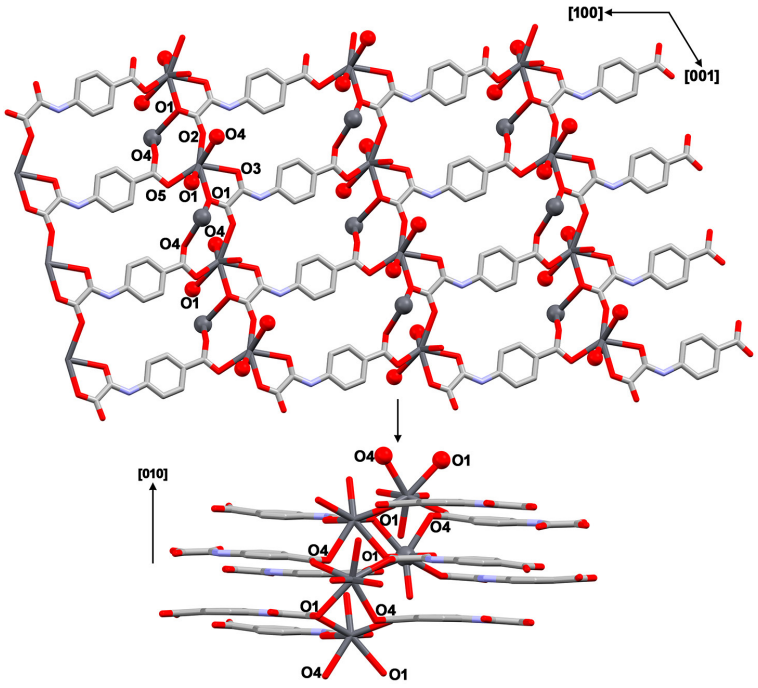

Figure 4. The three-dimensional coordination network assembled in the crystal structure of **2**. A two-dimensional sheet fragment (top), wherein Pb and O atoms responsible for its linkage to other sheet fragments (bottom) are depicted as grey and red balls, respectively. Some oxygen atoms are labelled for better comprehension.

from 200 to 800 nm (inset b in Figure 5) shows no other absorption features in other lower energy regions.

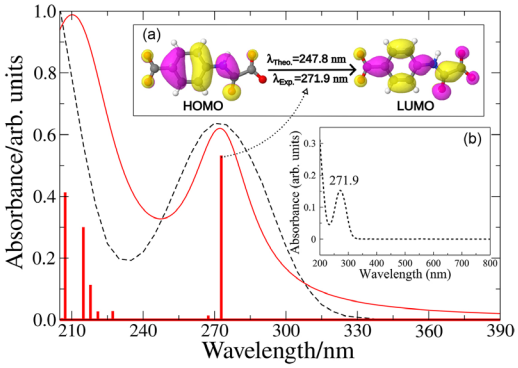

Figure 5. Experimental (dashed black line) and the convoluted theoretical (solid red line) UV-Vis spectra of the ligand in water. The red bars are the wavelength and the oscillator strength computed by TD-DFT. The inset (a) shows the HOMO-LUMO transition and (b) is the experimental UV-Vis recorded from 200-800 nm. Theoretical results were shifted by 25 nm to higher values of wavelength.

Diffuse reflectance (DR) spectra for **1**-**3** and for and for the Na_2Hpcpa ligand are depicted in Figures S6a-S6d (SI section), respectively. The spectra present the band edge absorption near 330-340 nm with reflectance greater than 90%. The similar characteristics of DR spectra **1**-**3** are expected since the compounds show similar structures. From the DR spectra and using the Kubelka-Munk theory,[57,58] the optical band gap (E_g) was determined and calculated from the $[F(R_\infty)hv]^2$ *vs.* hv plots (insets in Figures S6a-S6c), and the values of 3.84, 3.51 and 3.56 eV for **1**, **2** and **3**, respectively, are typical values of non-conducting materials, the detailed method description of E_g is presented in Supplementary Information section. The E_g for the gadolinium(III) compound, called here as **4**, was determined in our previous work,[46] being 3.52 eV, as well as those for Tb^{3+} and Eu^{3+} complexes, 3.43 and 3.61 eV, respectively. For Na_2Hpcpa ligand is found a E_g = 3.70 eV.

Excitation spectra of **1**-**4** and Na_2Hpcpa ligand were recorded by monitoring its corresponding emission bands (Figure 6a). They present similar spectral characteristics, consisting of wide bands between 260 and 390 nm. The emission spectra, Figure 6b, were collected under 330 nm excitation wavelength. All emission spectra consist of a broadband spread from the deep blue to the red region (360 to 650 nm) with maximum centered at ca. 452 nm (**1**) and 436 nm (**2**), 413 nm (**3**), 422 nm (**4**), and 410 nm Na_2Hpcpa. The narrow band in the emission spectrum of (**4**) is due to the Eu^{3+}. The observed red-shift in the position of the emission band could be attributed to the different crystalline field experienced by the different ions in their symmetry site due to the different coordination, changing the crystalline field and shift the emission position.[59] The CIE1931 colorimetric coordinates are shown in Figure 7 and Table 2. For Na_2Hpcpa the CIE values lie in the blue-deep color region, and for **1**-**4**

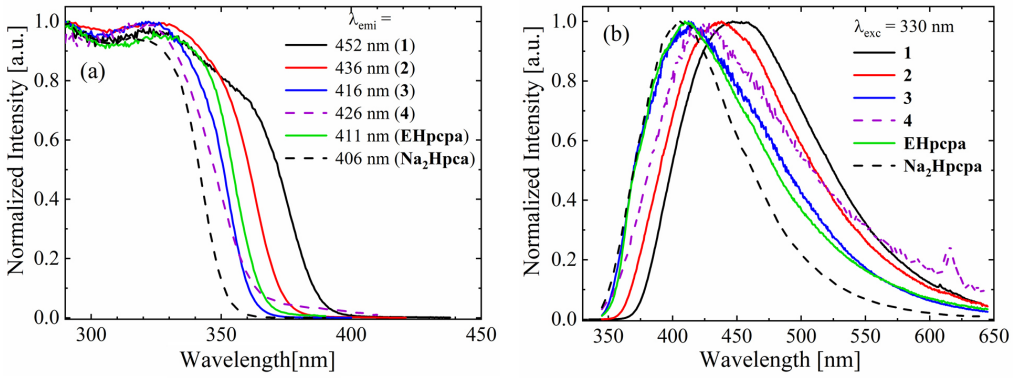

Figure 6. Room temperature excitation (a) and emission (b) spectra of **1**-**4** and proligand Na_2Hpcpa.

Table 2. Lifetime values, external and internal quantum yields and CIE(x,y) coordinate values for **1**-**4** and ligand Na_2Hpcpa

Sample	τ_1 / ns	τ_2 / ns	τ_{AV} / ns	iQY / %	eQY / %	CIE(x,y)
				λ_{exc} = 330 nm		
1	2.83(1)			18.6	15.4	(0.192, 0.220)
2	0.29(1) 99.0%	0.63(2) 1.0%	0.32	6.8	5.8	(0.188,0.188)
3	1.38(1)			15.0	12.8	(0.178, 0.159)
4	1.39(2)			0.15	0.13	(0.212, 0.210)
Na_2Hpcpa	2.68(4) 21.7%	6.52(5) 78.3 %	5.7	23.8	18.6	(0.164, 0.099)

τ_i and τ_{AV}: lifetime values; eQY: external; iQY: internal quantum yields; CIE(x,y): 1931 chromaticity coordinates.

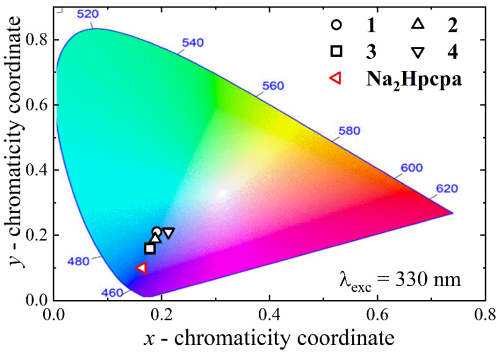

Figure 7. CIE 1931 color coordinates of the PL emission.

complexes is observed a shift in the CIE values in the chromaticity diagram reflecting the redshift observed in their emission band position, with CIE values following the order **3**-**2**-**1**-**4** from blue to white color.

The lifetime was evaluated from the luminescent decay curves (Figure 8), measured by monitoring the emissions at 452 nm (**1**), 436 nm (**2**), 413 nm (**3**), 422 nm (**4**) and 410 nm (Na_2Hpcpa). The lifetime values were calculated by fitting the decay curves with a mono-exponential function for **1**, **3** and **4** and with a bi-exponential function in the case of **2** and Na_2Hpcpa, $I(t)/I_0 = A_1\exp(-t/\tau_1) + A_2\exp(-t/\tau_2)$ and $\tau_{AV} = (A_1\tau_1^2 + A_2\tau_2^2)/(A_1\tau_1 + A_2\tau_2)$, where A_1 and A_2 are constants, τ_1 and τ_2 the decay time for the exponential component and $I(t)/I_0$ the normalized intensity, see Supplementary Information section for more details. The bi-exponential decay results indicate that two types of transitions are involved in the observed emissions, and have been related by Priya *et al.*[60] to the short and longer life times, corresponding to the different relaxation mechanisms. The best-fit values are listed in Table 2. The internal and external photoluminescence quantum yields (iQY and eQY, Table 2) reached maximum values of 15.4 (**1**), 5.8 (**2**), 15.0 (**3**) and 0.15% (**4**). An interesting eQY value of 18.6% for Na_2Hpcpa ligand was measured. A good correlation between the τ and QY values of **1**-**3** and the ligand is observed, indicating that these compounds experience similar mechanisms for quenching the luminescence. Moreover, these results show that despite the structural similarities between the metal complexes the lifetime decrease can be due to the non-radiative decay. Similar features were observed by Campos *et al.*[61] for the isostructural polymers of formula $[Cd(ampyz)(AcO)_2(H_2O)]_\infty$ and $[Zn(ampyz)(AcO)_2(H_2O)]_\infty$, and by Lemes *et al.*,[62] that attributes the lower lifetimes and QYs to a strong phonon coupling, i.e., when a photoluminescence emission center is coupled well to vibrational modes (phonons) of the complex structure the quantum yield is reduced, as a consequence of a fast depopulation of excited levels what lead a high non-radiative phonon-assisted relaxation rate.[63]

On the other hand, in comparing with Tb^{3+} and Eu^{3+} oxamate complexes $\{Ln^{III}_2(Hpcpa)_3(H_2O)_5\cdot H_2O\}_n$,[46] Eu(III) (iQY = 1.8%, eQY = 0.8%) and Tb^{3+} (iQY = 7.8%, eQY = 6.8%), where these values are due essentially to the narrow Ln^{3+} emission bands because their emission spectra do not present any band due the ligand, the greater eQY values obtained here for Cd and Zn complexes could be explained to their large ligand emission bands.

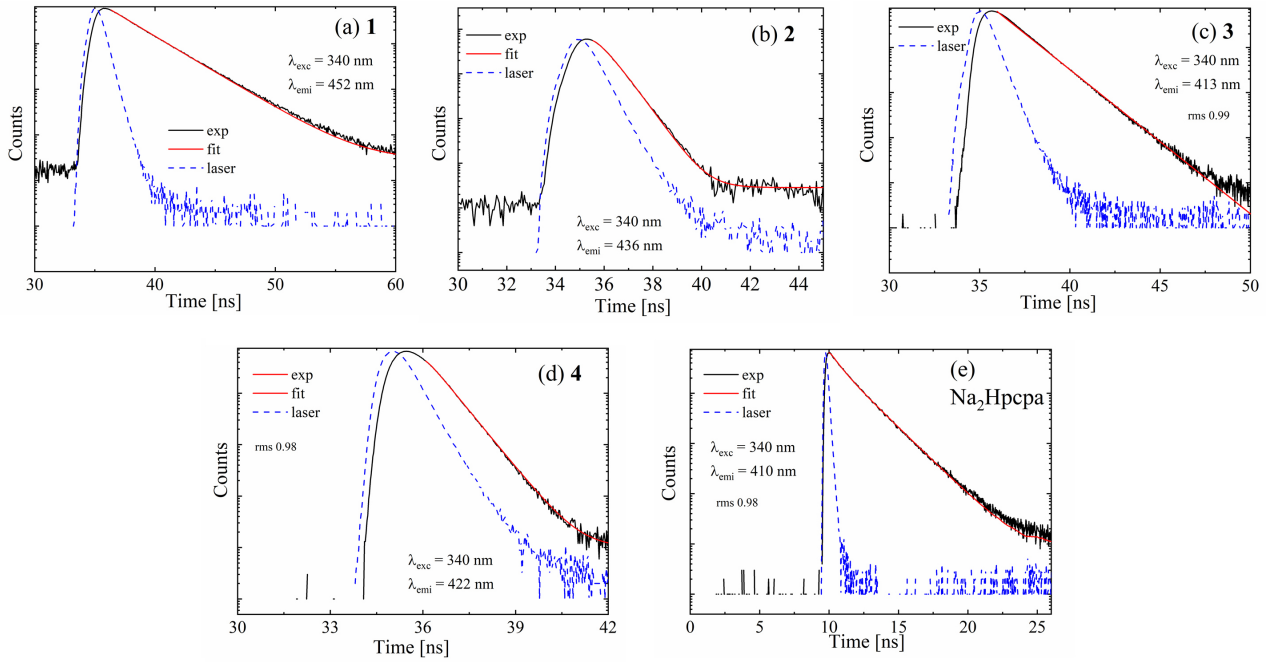

Figure 8. Excited state decay curves for **1**-**4** (a-d) and proligand Na_2Hpcpa (e).

Conclusions

In summary, the exploration of the rich coordination chemistry of the pcpa oxamato-type ligand has led to the successful preparation of two novel coordination polymers through its interaction with Cd(II) and Pb(II) ions in aqueous solution. These polymers constitute new additions to a series of pcpa-based coordination polymers previously reported by our group. Photoluminescence studies on selected members of this series demonstrated remarkably high values of external quantum yield (eQY) of up to 15.4%, with the Cd(II) polymer reported herein achieving the highest yield. These findings suggest that certain compounds within this series could be used as promising candidates for UV to visible light conversion in lighting devices, particularly those containing Cd(II) and Zn(II) ions. Furthermore, this series of coordination polymers illustrates well the great capability of the $Hpcpa^{2-}$ ligand in capturing metal ions from aqueous media. So, this work not only expands our understanding of oxamate coordination chemistry but also highlights the potential applications of these compounds in optoelectronic devices.

Supplementary Information

Crystallographic data, characterizations, diffuse reflectance spectra and emission spectra. CCDC 2102736 (**1**) and 2102735 (**2**) codes contain the supplementary crystallographic data for this paper. These data can be obtained free of charge via www.ccdc.cam.ac.uk/data_request/cif, by emailing data_request@ccdc.cam.ac.uk, or by contacting The Cambridge Crystallographic Data Centre, 12 Union Road, Cambridge CB2 1EZ, UK; fax: +44 1223 336033.

Supplementary information is available free of charge at http://jbcs.sbq.org.br as PDF file.

Acknowledgments

J. W. M. is grateful to CAPES for the doctoral grant. This study was financed by the CAPES, CNPq, FAPEG and FINEP Brazilian agencies. We are indebted to Prof Dr Paulo Sérgio de Souza and Dr Fabrício Ribeiro de Souza from Laboratório de Instrumentação Analítica (UFG) for their help with the atomic absorption spectroscopy measurements.

Author Contributions

Danielle Cangussu was responsible for conceptualization, investigation, project administration, supervision, writing (original draft, review and editing); Ricardo C. de Santana for conceptualization, data curation, formal analysis, writing (original draft, review and editing); Jhonny W. Maciel for conceptualization, data curation, formal analysis, investigation, methodology; Jackson Junior Santos de Souza for data curation, formal analysis, methodology; Ana Karoline S. M. Valdo for data curation, formal analysis; Felipe T. Martins for data curation, formal analysis, writing original draft; Freddy F. Guimaraes for formal analysis, methodology; Lauro J. Q. Maia for data curation, formal analysis, writing original draft.

References

1. Zheng, Y.-Z.; Zheng, Z.; Chen, X.-M.; *Coord. Chem. Rev.* **2014**, *258-259*, 1. [Crossref]
2. Leong, W. L.; Vittal, J. J.; *Chem. Rev.* **2011**, *111*, 688. [Crossref]
3. Nouar, F.; Devic, T.; Chevreau, H.; Guillou, N.; Gibson, E.; Clet, G.; Daturi, M.; Vimont, A.; Grenèche, J. M.; Breeze, M. I.; Walton, R. I.; Llewellyn, P. L.; Serre, C.; *Chem. Commun.* **2012**, *48*, 10237. [Crossref]
4. Zhang, Y.-B.; Furukawa, H.; Ko, N.; Nie, W.; Park, H. J.; Okajima, S.; Cordova, K. E.; Deng, H.; Kim, J.; Yaghi, O. M.; *J. Am. Chem. Soc* **2015**, *137*, 2641. [Crossref]
5. Wang, H.; Shi, Z.; Yang, J.; Sun, T.; Rungtaweevoranit, B.; Lyu, H.; Zhang, Y.; Yaghi, O. M.; *Angew. Chem., Int. Ed.* **2021**, *60*, 3417. [Crossref]
6. Ye, Y.; Ma, Z.; Lin, R.-B.; Krishna, R.; Zhou, W.; Lin, Q.; Zhang, Z.; Xiang, S.; Chen, B.; *J. Am. Chem. Soc.* **2019**, *141*, 4130. [Crossref]
7. Yu, L.; Ullah, S.; Zhou, K.; Xia, Q.; Wang, H.; Tu, S.; Huang, J.; Xia, H.-L.; Liu, X.-Y.; Thonhauser, T.; Li, J.; *J Am. Chem. Soc.* **2022**, *144*, 3766. [Crossref]
8. Cao, C.-C.; Chen, C.-X.; Wei, Z.-W.; Qiu, Q.-F.; Zhu, N.-X.; Xiong, Y.-Y.; Jiang, J.-J.; Wang, D.; Su, C.-Y.; *J. Am. Chem. Soc.* **2019**, *141*, 2589. [Crossref]
9. Kalaj, M.; Palomba, J. M.; Bentz, K. C.; Cohen, S. M.; *Chem. Commun.* **2019**, *55*, 5367. [Crossref]
10. Viciano-Chumillas, M.; Mon, M.; Ferrando-Soria, J.; Corma, A.; Leyva-Pérez, A.; Armentano, D.; Pardo, E.; *Acc. Chem. Res.* **2020**, *53*, 520. [Crossref]
11. Mon, M.; Bruno, R.; Tiburcio, E.; Viciano-Chumillas, M.; Kalinke, L. H. G.; Ferrando-Soria, J.; Armentano, D.; Pardo, E.; *J. Am. Chem. Soc.* **2019**, *141*, 13601. [Crossref]
12. Singha, D. K.; Majee, P.; Mondal, S. K.; Mahata, P.; *Polyhedron* **2019**, *158*, 277. [Crossref]
13. Mon, M.; Bruno, R.; Tiburcio, E.; Casteran, P.; Ferrando-Soria, J.; Armentano, D.; Pardo, E.; *Chem. - Eur. J.* **2018**, *24*, 17712. [Crossref]
14. Xia, W.; Mahmood, A.; Zou, R.; Xu, Q.; *Energy Environ. Sci.* **2015**, *8*, 1837. [Crossref]
15. Liang, Z.; Qu, C.; Guo, W.; Zou, R.; Xu, Q.; *Adv. Mater.* **2018**, *30*, 1702891. [Crossref]

16. Li, J.; Yuan, S.; Qin, J.; Pang, J.; Zhang, P.; Zhang, Y.; Huang, Y.; Drake, H. F.; Liu, W. R.; Zhou, H.; *Angew. Chem., Int. Ed.* **2020**, *59*, 9319. [Crossref]
17. Xu, R.; Wang, Y.; Duan, X.; Lu, K.; Micheroni, D.; Hu, A.; Lin, W.; *J. Am. Chem. Soc.* **2016**, *138*, 2158. [Crossref]
18. Gui, B.; Meng, Y.; Xie, Y.; Tian, J.; Yu, G.; Zeng, W.; Zhang, G.; Gong, S.; Yang, C.; Zhang, D.; Wang, C.; *Adv. Mater.* **2018**, *30*, 1802329. [Crossref]
19. Liu, Y.; Ma, Y.; Yang, J.; Diercks, C. S.; Tamura, N.; Jin, F.; Yaghi, O. M.; *J. Am. Chem. Soc.* **2018**, *140*, 16015. [Crossref]
20. Liu, J.-Q.; Luo, Z.-D.; Pan, Y.; Kumar Singh, A.; Trivedi, M.; Kumar, A.; *Coord. Chem. Rev.* **2020**, *406*, 213145. [Crossref]
21. Hu, Z.; Deibert, B. J.; Li, J.; *Chem. Soc. Rev.* **2014**, *43*, 5815. [Crossref]
22. Xu, L.-J.; Xu, G.-T.; Chen, Z.-N.; *Coord. Chem. Rev.* **2014**, *273-274*, 47. [Crossref]
23. Newsome, W. J.; Chakraborty, A.; Ly, R. T.; Pour, G. S.; Fairchild, D. C.; Morris, A. J.; Uribe-Romo, F. J.; *Chem. Sci.* **2020**, *11*, 4391. [Crossref]
24. Lustig, W. P.; Shen, Z.; Teat, S. J.; Javed, N.; Velasco, E.; O'Carroll, D. M.; Li, J.; *Chem. Sci.* **2020**, *11*, 1814. [Crossref]
25. Chen, C.-X.; Qiu, Q.-F.; Pan, M.; Cao, C.-C.; Zhu, N.-X.; Wang, H.-P.; Jiang, J.-J.; Wei, Z.-W.; Su, C.-Y.; *Chem. Commun.* **2018**, *54*, 13666. [Crossref]
26. Jia, J.; Gutiérrez-Arzaluz, L.; Shekhah, O.; Alsadun, N.; Czaban-Jóźwiak, J.; Zhou, S.; Bakr, O. M.; Mohammed, O. F.; Eddaoudi, M.; *J. Am. Chem. Soc.* **2020**, *142*, 8580. [Crossref]
27. Zhu, D.; Zhang, Y.; Bao, S.; Wang, N.; Yu, S.; Luo, R.; Ma, J.; Ju, H.; Lei, J.; *J. Am. Chem. Soc.* **2021**, *143*, 3049. [Crossref]
28. Edelmann, F. T.; *Chem. Soc. Rev.* **2012**, *41*, 7657. [Crossref]
29. Werner, E. J.; Datta, A.; Jocher, C. J.; Raymond, K. N.; *Angew. Chem., Int. Ed.* **2008**, *47*, 8568. [Crossref]
30. Lian, X.; Zhao, D.; Cui, Y.; Yang, Y.; Qian, G.; *Chem. Commun.* **2015**, *51*, 17676. [Crossref]
31. Wang, Z.; Ananias, D.; Carné-Sánchez, A.; Brites, C. D. S.; Imaz, I.; Maspoch, D.; Rocha, J.; Carlos, L. D.; *Adv. Funct. Mater.* **2015**, *25*, 2824. [Crossref]
32. Cui, Y.; Zhu, F.; Chen, B.; Qian, G.; *Chem. Commun.* **2015**, *51*, 7420. [Crossref]
33. Feng, T.; Ye, Y.; Liu, X.; Cui, H.; Li, Z.; Zhang, Y.; Liang, B.; Li, H.; Chen, B.; *Angew. Chem., Int. Ed.* **2020**, *132*, 21936. [Crossref]
34. Kaczmarek, A. M.; Liu, Y.; Kaczmarek, M. K.; Liu, H.; Artizzu, F.; Carlos, L. D.; Van Der Voort, P.; *Angew. Chem., Int. Ed.* **2020**, *59*, 1932. [Crossref]
35. Liu, Y.; Pan, M.; Yang, Q.-Y.; Fu, L.; Li, K.; Wei, S.-C.; Su, C.-Y.; *Chem. Mater.* **2012**, *24*, 1954. [Crossref]
36. Li, L.; Cheng, J.; Liu, Z.; Song, L.; You, Y.; Zhou, X.; Huang, W.; *ACS Appl. Mater. Interfaces* **2018**, *10*, 44109. [Crossref]
37. Singha, D. K.; Bhattacharya, S.; Majee, P.; Mondal, S. K.; Kumar, M.; Mahata, P.; *J. Mater. Chem. A* **2014**, *2*, 20908. [Crossref]
38. Singha, D. K.; Majee, P.; Mondal, S. K.; Mahata, P.; *Eur. J. Inorg. Chem.* **2015**, *2015*, 1390. [Crossref]
39. Xia, T.; Zhu, F.; Jiang, K.; Cui, Y.; Yang, Y.; Qian, G.; *Dalton Trans.* **2017**, *46*, 7549. [Crossref]
40. Ye, J.-W.; Lin, J.-M.; Mo, Z.-W.; He, C.-T.; Zhou, H.-L.; Zhang, J.-P.; Chen, X.-M.; *Inorg. Chem.* **2017**, *56*, 4238. [Crossref]
41. Ferrando-Soria, J.; Pasán, J.; Ruiz-Pérez, C.; Journaux, Y.; Julve, M.; Lloret, F.; Cano, J.; Pardo, E.; *Inorg. Chem.* **2011**, *50*, 8694. [Crossref]
42. Grancha, T.; Acosta, A.; Cano, J.; Ferrando-Soria, J.; Seoane, B.; Gascon, J.; Pasán, J.; Armentano, D.; Pardo, E.; *Inorg. Chem.* **2015**, *54*, 10834. [Crossref]
43. Ferrando-Soria, J.; Grancha, T.; Julve, M.; Cano, J.; Lloret, F.; Journaux, Y.; Pasán, J.; Ruiz-Pérez, C.; Pardo, E.; *Chem. Commun.* **2012**, *48*, 3539. [Crossref]
44. Oliveira, T. L.; Kalinke, L. H. G.; Mascarenhas, E. J.; Castro, R.; Martins, F. T.; Sabino, J. R.; Stumpf, H. O.; Ferrando, J.; Julve, M.; Lloret, F.; Cangussu, D.; *Polyhedron* **2014**, *81*, 105. [Crossref]
45. Maciel, J. W.; Kalinke, L. H. G.; Valdo, A. K.; Martins, F. T.; Rabelo, R.; Moliner, N.; Cano, J.; Julve, M.; Lloret, F.; Cangussu, D.; *J. Braz. Chem. Soc.* **2019**, *30*, 2413. [Crossref]
46. Maciel, J. W. O.; Lemes, M. A.; Valdo, A. K.; Rabelo, R.; Martins, F. T.; Queiroz Maia, L. J.; de Santana, R. C.; Lloret, F.; Julve, M.; Cangussu, D.; *Inorg. Chem.* **2021**, *60*, 6176. [Crossref]
47. Sheldrick, G. M.; *Acta Crystallogr., Sect. C: Struct. Chem.* **2015**, *71*, 3. [Crossref]
48. Macrae, C. F.; Sovago, I.; Cottrell, S. J.; Galek, P. T. A.; McCabe, P.; Pidcock, E.; Platings, M.; Shields, G. P.; Stevens, J. S.; Towler, M.; Wood, P. A.; *J. Appl. Cryst.* **2020**, *53*, 226. [Crossref]
49. Farrugia, L. J.; *ORTEP-3*, School of Chemistry, University of Glasgow, Glasgow, Scotland, 2012.
50. Wrighton, M. S.; Ginley, D. S.; Morse, D. L.; *J. Phys. Chem.* **1974**, *78*, 2229. [Crossref]
51. Wyman, C.; Sloan, P.-P.; Shirley, P.; *J. Computer Graphics Techniques* **2013**, *2*, 1. [Link] accessed in April 2024
52. Tomasi, J.; Mennucci, B.; Cammi, R.; *Chem. Rev.* **2005**, *105*, 2999. [Crossref]
53. Zhao, Y.; Truhlar, D. G.; *Theor. Chem. Acc.* **2008**, *120*, 215. [Crossref]
54. Weigend, F.; Ahlrichs, R.; *Phys. Chem. Chem. Phys.* **2005**, *7*, 3297. [Crossref]
55. Weigend, F.; *Phys. Chem. Chem. Phys.* **2006**, *8*, 1057. [Crossref]
56. Frisch, M. J.; Frisch, M. J.; Trucks, G. W.; Schlegel, H. B.; Scuseria, G. E.; Robb, M. A.; Cheeseman, J. R.; Scalmani, G.; Barone, V.; Petersson, G. A.; Nakatsuji, H.; Li, X.; Caricato, M.; Marenich, A. V.; Bloino, J.; Janesko, B. G.; Gomperts, R.; Mennucci, B.; Hratchian, H. P.; Ortiz, J. V.; Izmaylov, A. F.; Sonnenberg, J. L.; Williams; Ding, F.; Lipparini, F.; Egidi, F.;

Goings, J.; Peng, B.; Petrone, A.; Henderson, T.; Ranasinghe, D.; Zakrzewski, V. G.; Gao, J.; Rega, N.; Zheng, G.; Liang, W.; Hada, M.; Ehara, M.; Toyota, K.; Fukuda, R.; Hasegawa, J.; Ishida, M.; Nakajima, T.; Honda, Y.; Kitao, O.; Nakai, H.; Vreven, T.; Throssell, K.; Montgomery Jr., J. A.; Peralta, J. E.; Ogliaro, F.; Bearpark, M. J.; Heyd, J. J.; Brothers, E. N.; Kudin, K. N.; Staroverov, V. N.; Keith, T. A.; Kobayashi, R.; Normand, J.; Raghavachari, K.; Rendell, A. P.; Burant, J. C.; Iyengar, S. S.; Tomasi, J.; Cossi, M.; Millam, J. M.; Klene, M.; Adamo, C.; Cammi, R.; Ochterski, J. W.; Martin, R. L.; Morokuma, K.; Farkas, O.; Foresman, J. B.; Fox, D. J.; *Gaussian 16*, Revision B.01; Gaussian, Inc., Wallingford CT, 2016.

57. Kubelka, P.; Munk, F.; *Zeitschrift Für Tech. Phys*. **1931**, *12*, 593. [Link] accessed in April 2024
58. Adachi, C.; Baldo, M. A.; Forrest, S. R.; *J. Appl. Phys.* **2000**, *87*, 8049. [Crossref]
59. Solé, J. G.; Bausá, L. E.; Jaque, D.; *An Introduction to the Optical Spectroscopy of Inorganic Solids*; Wiley: Chichester, England, 2005.
60. Priya, J.; Gondia, N. K.; Kunti, A. K.; Sharma, S. K.; *ECS J. Solid State Sci. Technol.* **2016**, *5*, R166. [Crossref]
61. Campos, J. H. D.; Alvarenga, M. E.; Lemes, M. A.; do Nascimento Neto, J. A.; Guimarães, F. F.; Maia, L. J.; de Santana, R. C. Q.; Martins, F. T.; *Dyes Pigm.* **2021**, *186*, 109025. [Crossref]
62. Lemes, M. A.; do Nascimento Neto, J. A.; Fernandes Guimarães, F.; Maia, L. J. Q.; de Santana, R. C.; Terra Martins, F.; *New J. Chem.* **2020**, *44*, 20259. [Crossref]
63. Hamze, R.; Peltier, J. L.; Sylvinson, D.; Jung, M.; Cardenas, J.; Haiges, R.; Soleilhavoup, M.; Jazzar, R.; Djurovich, P. I.; Bertrand, G.; Thompson, M. E.; *Science* **2019**, *363*, 601. [Crossref]

Submitted: February 9, 2024
Published online: May 7, 2024